Available online at www.sciencedirect.com
SCIENCE DIRECT®
Nuclear Engineering and Design 229 (2004) 189–197
Nuclear Engineering and Design
www.elsevier.com/locate/nucengdes

Elasto-plastic behavior of pipe subjected to steady axial load and cyclic bending

Yanping Yao [a,*], Ming-Wan Lu [b], Xiong Zhang [b]

[a] *Department of OffShore Engineering, China Classification Society, A Bldg Century Square, 99 Wangfujing Avenue, Beijing 100006, PR China*
[b] *Departmernt of Engineering Mechanics, Tsinghua University, Beijing 100084, PR China*

Received 12 October 2001; received in revised form 23 August 2003; accepted 25 October 2003

Abstract

The elasto-plastic behavior of a pipe subjected to a steady axial force and a cyclic bending moment is studied. By using two parameters *c* and *d*, which describe the elasto-plastic interfaces of beam cross-section, the boundary curve equations between various types of elasto-plastic behavior, such as shakedown, plastic fatigue, ratcheting, and plastic collapse, are derived. The results are applicable for beams of any cross-section with two orthogonal axes of symmetry. As a result, the load regime diagram for a pipe is obtained, which gives an intuitive picture of the elasto-plastic behavior of the pipe under a given combination of constant axial load and cyclic bending moment.
© 2003 Elsevier B.V. All rights reserved.

1. Introduction

Piping systems play an important role in many applications, especially in nuclear power plants. The dynamic design, including seismic design is a key part of modern piping design and analysis (Slagis, 1991). The criteria of piping design given by the ASME Boiler and Pressure Vessel Code, Section III and VIII-2, is based on linear elastic analysis. This analysis method has proved to be too conservative in practice and in many experimental studies since the 1980s (Slagis, 1996; PVRC Subcommittee, 1994). The EPRI/NRC Piping and Fitting Dynamic Reliability Test Program showed that the failure mode of piping components subjected to large seismic loading is not collapse, as in the static case, but fatigue or fatigue-ratcheting (Tagart et al., 1990). Therefore, the fatigue and ratcheting analysis of piping that is subjected to seismic or other cyclic loads is very important for predicting the dynamic response and lifespan of piping. Scavuzzo et al. (1991, 1992) have done valuable work on the ratcheting analysis of pressurized pipe subjected to cyclic bending loads. They found that depending upon loading conditions and specified material properties, three different responses were observed from the finite element analyses: cyclic plasticity, ratcheting of the hoop strain, or shakedown. These analytical results are compared to some experimental measurements. Hassan et al. (1998) obtained good results in the prediction of the incremental hoop ratchet strain of pressurized pipes subjected to dynamic loading. The focus of these studies was confined to the numerical and experimental analysis of ratcheting, one of the inelastic failure modes. In this paper, we put emphasis on the limiting loading conditions for different types of elasto-plastic behavior, such as shakedown, ratcheting, and plastic fatigue,

* Corresponding author. Tel.: +86-10-65136633x337; fax: +86-10-65246824.
E-mail address: yaoyp@ccs.org.cn (Y. Yao).

0029-5493/$ – see front matter © 2003 Elsevier B.V. All rights reserved.
doi:10.1016/j.nucengdes.2003.10.013

Nomenclature

A, B_1, B_2, B_3, B_4	coefficients of polynomial regression
Loads	
M	amplitude of cyclic bending moment
M_e	elastic limit load of bending moment amplitude
m, M/M_e	dimensionless bending moment amplitude
N	steady axial force
N_e	elastic limit load of axial force
n, N/N_e	dimensionless axial force
Geometrical parameters	
A	area of the cross-section
a, b, a_1, b_1, a_2, b_2	elastic–plastic interfaces of beam cross-section during moment application and reversal
c, d	distance from zero-stress line to the elastic–plastic interface and to the center line of the beam, respectively
R	half-depth of the beam, outer radius of the pipe
r	inner radius of the pipe
α	ratio of inner to outer radius of the pipe
β	section shape coefficient
λ_c	c/R dimensionless distance
λ_d	d/R dimensionless distance
κ, κ_1, κ_2	curvature of the beam during moment application and reversal
Physical parameters	
E	elastic modulus
I_z	inertial moment
σ_y	yield stress
σ_n, N/A	axial stress caused by axial force N
σ_m, MR/I_z	axial stress caused by bending moment amplitude M
σ	stress distribution on the beam cross-section
ε_i^p, $\varepsilon_i^{p'}$	plastic strain when moment application and reversal during the ith cycle
η_i,η_i'	the increment of plastic strain during the ith moment application and reversal

etc., which are an important basis of the inelastic dynamic evaluation of piping.

A pipe under seismic excitation is simplified as an elastic-perfectly-plastic beam with tubular cross-section subjected to steady axial force and fully reversed cyclic bending moment. Yu and Johnson (1982) examined the elastic-perfectly-plastic behavior of a rectangular beam subjected to different combinations of static axial tension and bending. Webster et al. (1985) studied the same problem but with fully reversed cyclic bending and gave a load regime diagram identical to the "shakedown" diagram derived by Gokhfeld and Cherniavsky (1980). In the present paper, the boundary curve equations between various load regimes are derived by introducing two parameters c and d, which indicate the interfaces of the elastic and plastic region on the beam cross-section. The results are applicable for beams with biaxial symmetric cross-section that are loaded in their symmetry planes. A biaxial symmetric cross-section has two orthogonal axes of symmetry, as shown in Fig. 1.

In the following investigation, the assumptions of classical beam theory are adopted. The deflection of the beam axis is assumed to be small compared to the cross-sectional dimensions of the beam, and the cross-section is assumed to remain plane and normal to the deformed beam axis. During cyclic loading, effects due to cyclic hardening and ovalization are assumed to be negligible.

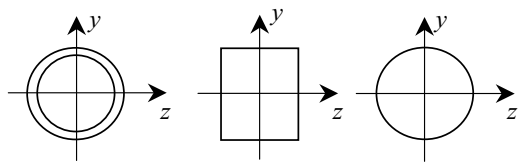

Fig. 1. Several examples of biaxial symmetric cross-sections of a beam.

2. Behavior classification and boundary curve equations of load regime diagram

2.1. Behavior classification

The following discussion focuses on the limiting conditions of various types of elasto-plastic behavior and the corresponding stress and strain distributions.

For different combinations of a static axial force N and a bending moment M, four kinds of elasto-plastic behavior are possible after the first 1/4 loading cycle (Yu and Johnson, 1982): (a) elastic, (b) one-sided plastic, (c) two-sided plastic, (d) plastic collapse, as shown in Fig. 2.

In Fig. 2, the two parameters c and d introduced by Yu and Johnson (1982) are used, which are the distance from the zero-stress line to the elastic–plastic interface and to the center line, respectively. The stress distributions characterized by c and d should satisfy the equilibrium conditions:

$$N = \int_A \sigma \, \mathrm{d}A; \quad M = \int_A \sigma y \, \mathrm{d}A \tag{1}$$

where A is the area of the cross-section. For given N and M, the parameters c and d are determined by Eq. (1). Fig. 2 shows that one-sided plasticity, two-sided plasticity, and plastic collapse correspond to the conditions $c + d > R$, $c + d \leq R$, and $c = 0$, respectively, where R is half-depth of the beam.

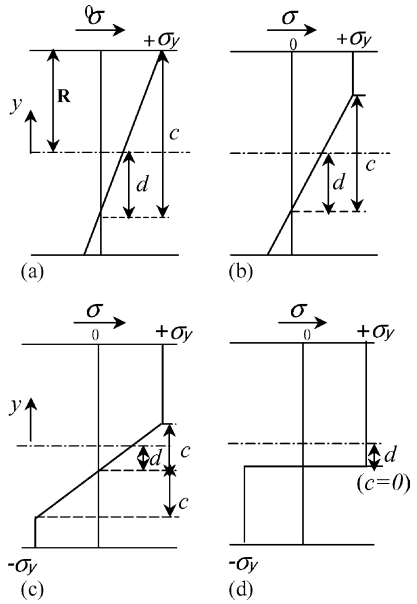

Fig. 2. Stress distributions across the section of a beam after first moment application. (a) Elastic; (b) one-sided plastic; (c) two-sided plastic; (d) plastic collapse.

After the first 1/4 loading cycle (equivalent to static loading), the bending moment will be fully reversed between M and $-M$. Various types of elasto-plastic behavior of a beam under steady axial force and cyclic bending moment will be discussed below. Using Bree's familiar notation (Bree, 1967, 1989), the load regime diagram is divided into various regions, i.e. elastic (E), shakedown (S), plastic fatigue (P), ratcheting (R), and plastic collapse (C_p).

2.1.1. Elastic region (E)

Elasticity governs until the maximum stress in the beam reaches the yield stress σ_y. The limiting condition for elastic region is:

$$|\sigma_n \pm \sigma_m| \leq \sigma_y \tag{2}$$

where $\sigma_n = N/A$ and $\sigma_m = MR/I_z$ are the axial stress and bending stress of the beam, respectively.

2.1.2. Shakedown region (S_1)

Shakedown refers to the case that further plastic deformation does not occur after a few initial cycles. We consider the one-sided plasticity case after the first 1/4 loading cycle, see Fig. 2b. For this case $\sigma_n + \sigma_m \geq \sigma_y$ at the upper plastic side, and $c + d > R$. Furthermore, if $c \geq d$ and $\sigma_m \leq \sigma_y$, i.e. the elasto-plastic interface does not exceed the center line of the cross-section, compressive yielding will not occur in the upper half while tensile yielding occurs in the lower half after the reversal of the moment, as shown in Fig. 3b. The whole section will remain elastic in later reloading

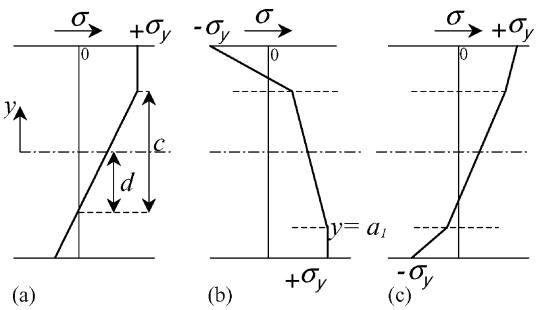

Fig. 3. Stress distributions of region S_1. (a) First moment application; (b) moment fully reversed; (c) second moment application.

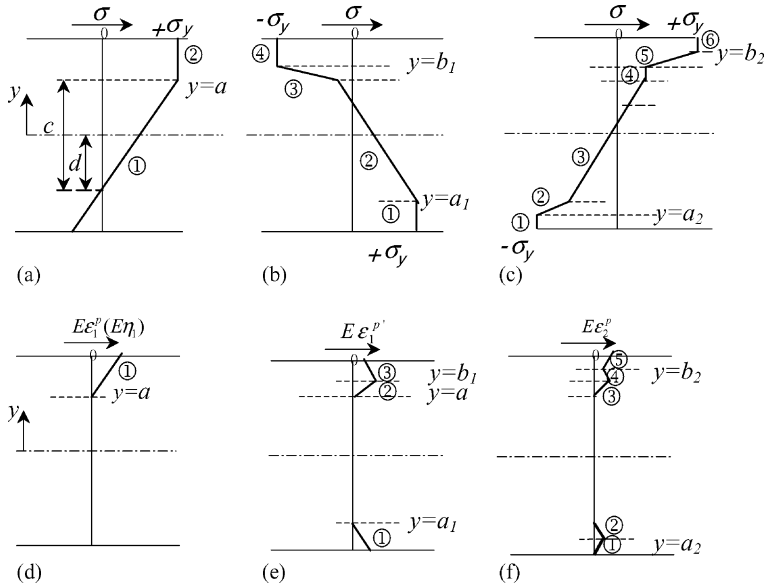

Fig. 4. Stress and strain distributions for region P_1. (a)–(c) Stress distributions; (d)–(f) plastic strain distributions.

and unloading cycles. The stress distribution repeats again and again between Fig. 3b and c. The beam has shaken down to elastic action.

The limiting conditions of the S_1 region are:

$$\sigma_n + \sigma_m \geq \sigma_y; \quad c + d \geq R; \quad c \geq d; \quad \sigma_m \leq \sigma_y$$

2.1.3. Cyclic plasticity region (P_1)

Consider the one-sided plasticity case, shown in Fig. 2b again, in which $\sigma_n + \sigma_m \geq \sigma_y$, $c + d > R$, and $c \geq d$, but $\sigma_m > \sigma_y$ now. In this case, compressive yielding will occur in the upper half during the reversal of the moment, as shown in Fig. 4b.

Introduce two parameters:

$$a = c - d; \quad E\kappa = \frac{\sigma_y}{c} \tag{3}$$

where E is the elastic modulus, κ is the curvature of the beam, and $E\kappa$ represents the slope of the stress distribution in Fig. 4a, see Eq. (4). In the same way, a_1, b_1, κ_1 and a_2, b_2, κ_2 were introduced in Fig. 4b and c, see Eqs. (5) and (6), which represent the stress distributions during the reversal and the reloading of the moment. The stress distributions must satisfy the equilibrium conditions Eq. (1). Through this and the continuity condition of the stress distribution, the parameters a_i, b_i, κ_i $(i = 1, 2)$ can be determined. By using the constitutive relationship for an elastic-perfectly-plastic material and the plane section hypothesis referred to above, we can obtain the corresponding plastic strain distributions as Fig. 4d–f shows, in which ε_i^p and $\varepsilon_i^{p'}$ are the plastic strain during moment application $(+M)$ and reversal $(-M)$ at the ith cycle, respectively. It can be proved that the stress and strain distributions will come back to Fig. 4b and e during the second reversal of the moment. Thus, Fig. 4b and c represents the stress distributions of a steady cycle.

The equations of the numbered curves in Fig. 4 are as follows:

Fig. 4a:

$$①\sigma = E\kappa(y - a) + \sigma_y; \quad ②\sigma = \sigma_y \tag{4}$$

Fig. 4b:

$$①\sigma = \sigma_y; \quad ②\sigma = E\kappa_1(y - a_1) + \sigma_y;$$
$$③\sigma = E(\kappa_1 - \kappa)(y - b_1) - \sigma_y; \quad ④\sigma = -\sigma_y \tag{5}$$

Fig. 4c:

$$①\sigma = -\sigma_y; \quad ②\sigma = E(\kappa_2 - \kappa_1)(y - a_2) - \sigma_y;$$
$$③\sigma = E\kappa_2(y - a_1) + E(\kappa_2 - \kappa_1)(a_1 - a_2) - \sigma_y;$$
$$④\sigma = E(\kappa_2 - \kappa)(y - b_1) + E(\kappa_2 - \kappa_1)(b_1 - b_2) + \sigma_y;$$
$$⑤\sigma = E(\kappa_2 - \kappa_1)(y - b_2) + \sigma_y; \quad ⑥\sigma = \sigma_y \tag{6}$$

Fig. 4d:

$$① E\varepsilon_1^p = E\kappa(y-a) \tag{7}$$

Fig. 4e:

$$① E\varepsilon_1^{p'} = E\kappa_1(y-a_1); \quad ② E\varepsilon_1^{p'} = E\kappa(y-a);$$
$$③ E\varepsilon_1^{p'} = E\kappa_1(y-b_1) + E\kappa(b_1-a) \tag{8}$$

Fig. 4f:

$$① E\varepsilon_2^p = E\kappa_2(y-a_2) + E\kappa_1(a_2-a_1);$$
$$② E\varepsilon_2^p = E\kappa_1(y-a_1); \quad ③ E\varepsilon_2^p = E\kappa(y-a);$$
$$④ E\varepsilon_2^p = E\kappa_1(y-b_1) + E\kappa(b_1-a);$$
$$⑤ E\varepsilon_2^p = E\kappa_2(y-b_2) + E\kappa_1(b_2-b_1) + E\kappa(b_1-a) \tag{9}$$

In the two regions of $y \geq b_2$ and $y \leq a_2$ in Fig. 4c, The same amount of plastic strain occurred with opposite sign during the application and reversal of the moment. The total plastic strain after one steady cycle is equal to zero, and therefore, the limiting conditions of the cyclic plasticity region P_1 are:

$$\sigma_n + \sigma_m \geq \sigma_y; \quad c + d \geq R; \quad c \geq d; \quad \sigma_m \geq \sigma_y$$

2.1.4. Ratcheting region (R_1)

Ratcheting is defined as the accumulation of plastic deformation with load cycles. There is a constant increment of plastic strain during every steady cycle of ratcheting.

When $c \leq d$, the tensile yielding zone exceeds the center line of the section during the first moment application, as shown in Fig. 5a. During the moment reversal, yield initially occurs in the zone $a \leq y \leq 0$ and then spreads further. The final stress distribution equilibrating with the axial load and moment is a mirror image of Fig. 5a, as shown in Fig. 5b. The stress distributions for further reversals of moment from $-M$ to $+M$ and from $+M$ to $-M$, are the same as those for the first cycle. The corresponding strain distributions are shown in Fig. 5d–f. The equations of the numbered strain distributions in Fig. 5d–f are as follows:

Fig. 5d:

$$① E\varepsilon_1^p = E\kappa(y-a) \tag{10}$$

Fig. 5e:

$$① E\varepsilon_1^{p'} = -2E\kappa a; \quad ② E\varepsilon_1^{p'} = E\kappa(y-a) \tag{11}$$

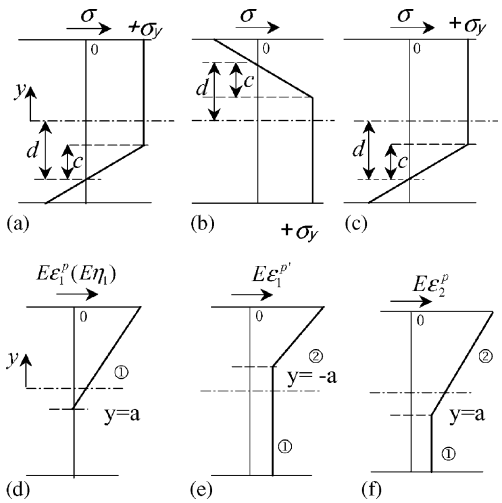

Fig. 5. Stress and strain distributions for region R_1. (a)–(c) Stress distributions; (d)–(f) plastic strain distributions.

Fig. 5f:

$$① E\varepsilon_2^p = -2E\kappa a; \quad ② E\varepsilon_2^p = E\kappa(y-a) - 2E\kappa a \tag{12}$$

$$\text{Define } \eta_i = \varepsilon_i^p - \varepsilon_{i-1}^{p'}; \quad \eta_i' = \varepsilon_i^{p'} - \varepsilon_i^p \tag{13}$$

as the increments of plastic strain during the ith moment application and reversal. The total strain increment per steady cycle is:

$$\delta = \eta_1' + \eta_2 = -2\kappa a \tag{14}$$

δ is called ratcheting strain, which is homogeneous through the cross-section.

The limiting conditions of the one-sided ratcheting region R_1 are:

$$c + d \geq R; \quad c \leq d$$

2.1.5. Shakedown region (S_2)

When $c + d \leq R$, two-sided yielding occurs close to the surfaces of the beam after the first moment application, as shown in Fig. 2c.

If $c \geq d$ and $\sigma_m \leq \sigma_y$, the whole cross-section will remain elastic during subsequent unloading and reloading cycles. The beam has shaken down. For a pipe, the intersection of these conditions will be null and shakedown region S_2 does not exist.

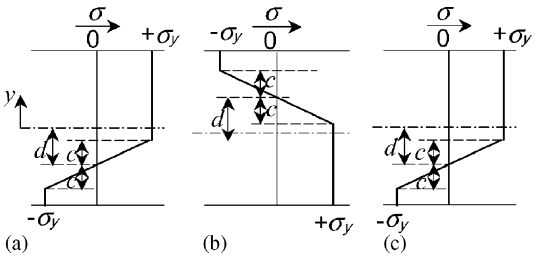

Fig. 6. Stress distributions for region R_2.

2.2. Reverse plasticity region (P_2)

If $c+d \le R$ and $c \ge d$, but $\sigma_m > \sigma_y$, similar steady stress and strain distributions as those of the region P_1 can be obtained, but compressive yielding occurs in the lower half of the beam during the first moment application.

The limiting conditions of the reverse plasticity region P_2 are:

$$c + d \le R; \quad c \ge d; \quad \sigma_m \ge \sigma_y$$

2.2.1. Ratcheting region (R_2)

If $c \le d$, the stress distribution after the first moment application is shown in Fig. 6a. Similar to region R_1, the stress distribution after reversal of the moment is a mirror image of Fig. 6a, as shown in Fig. 6b.

The limiting conditions of the ratcheting region R_2 are:

$$c + d \le R; \quad c \le d$$

2.2.2. Plastic collapse region (C_p)

When whole section yielding occurs during the first moment application, infinite plastic flow takes place, and the beam collapses. From Fig. 2d, the collapse condition can be expressed by $c = 0$.

2.3. Boundary curve equations of the load regime diagram

Introduce the following dimensionless variables:

$$\lambda_c = \frac{c}{R}, \quad \lambda_d = \frac{d}{R}, \quad m = \frac{M}{M_e}, \quad n = \frac{N}{N_e} \qquad (15)$$

where N_e and M_e are the elastic limit load under an axial force N and under a bending moment M, respectively. Using the dimensionless variables, the boundary curve equations between various regions mentioned above become:

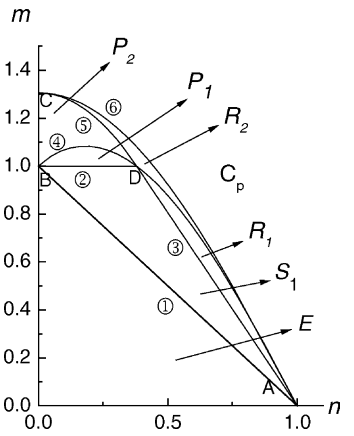

Fig. 7. Load regime diagram for the pipe ($\alpha = 0.95$).

E vs. S_1	$n + m = 1$	①
S_1 vs. P_1	$m = 1$	②
S_1 vs. R_1	$\lambda_c = \lambda_d$	③
P_1 vs. P_2 and R_1 vs. R_2	$\lambda_c + \lambda_d = 1$	④
P_2 vs. R_2	$\lambda_c = \lambda_d$	⑤
C_p vs. R_2	$\lambda_c = 0$	⑥

All of the Eqs. ①–⑥ are expressed in terms of n, m, and parameters λ_c, λ_d. Using Eq. (1), λ_c, λ_d can be determined by n, m. Plotting the curves of Eqs. ①–⑥ on the load plane n–m, we can obtain a *load regime diagram*. For the cross-section of a pipe, the load regime diagram is derived in following Section 3 and is shown in Fig. 7.

3. Load regime diagram for a pipe

3.1. Analytical formulation

Eqs. ①–⑥ are applicable to beams of any cross-section shape with two orthogonal axes of symmetry. Moreover, Eq. (1) is dependent on the particular shape of the cross-section. In this section, we focus on a pipe. For a round tube we have

$$N_e = \pi(1-\alpha^2)\sigma_y R^2; \quad M_e = \frac{\pi}{4}(1-\alpha^4)\sigma_y R^3 \qquad (16)$$

where α is ratio of inner to outer radius of the pipe.

For the case Fig. 2b, Eq. (1) becomes

$$
\begin{aligned}
N &= \left(\int_{c-d}^{R}\sigma_y \times 2\sqrt{R^2-y^2}\,\mathrm{d}y - \int_{c-d}\sigma_y \times 2\sqrt{r^2-y^2}\,\mathrm{d}y\right)\\
&\quad + \left(\int_{-R}^{c-d}\frac{\sigma_y}{c}(y+d)\times 2\sqrt{R^2-y^2}\,\mathrm{d}y - \int_{-r}^{c-d}\frac{\sigma_y}{c}(y+d)\times 2\sqrt{r^2-y^2}\,\mathrm{d}y\right);\\
M &= \left(\int_{c-d}^{R}\sigma_y y \times 2\sqrt{R^2-y^2}\,\mathrm{d}y - \int_{c-d}\sigma_y y \times 2\sqrt{r^2-y^2}\,\mathrm{d}y\right)\\
&\quad + \left(\int_{-R}^{c-d}\frac{\sigma_y}{c}(y+d)y\times 2\sqrt{R^2-y^2}\,\mathrm{d}y - \int_{-r}^{c-d}\frac{\sigma_y}{c}(y+d)y\times 2\sqrt{r^2-y^2}\,\mathrm{d}y\right)
\end{aligned}
\tag{17}
$$

After integration we obtain:

$$
\begin{aligned}
n\pi(1-\alpha^2) &= \left(\frac{\lambda_d}{\lambda_c}-1\right)(\lambda_c-\lambda_d)(\sqrt{1-(\lambda_c-\lambda_d)^2}-\sqrt{\alpha^2-(\lambda_c-\lambda_d)^2})\\
&\quad + \left(\frac{\lambda_d}{\lambda_c}-1\right)\left[\arcsin(\lambda_c-\lambda_d)-\alpha^2\arcsin\left(\frac{\lambda_c-\lambda_d}{\alpha}\right)\right] + \left(\frac{\lambda_d}{\lambda_c}+1\right)\left(\frac{\pi}{2}-\frac{\pi\alpha^2}{2}\right)\\
&\quad -\frac{2}{3\lambda_c}[(1-(\lambda_c-\lambda_d)^2)^{3/2}-(\alpha^2-(\lambda_c-\lambda_d)^2)^{3/2}];\\
\frac{m\pi}{4}(1-\alpha^4) &= \frac{2}{3}\left(1-\frac{\lambda_d}{\lambda_c}\right)[(1-(\lambda_c-\lambda_d)^2)^{3/2}-(\alpha^2-(\lambda_c-\lambda_d)^2)^{3/2}]\\
&\quad +\frac{1}{4\lambda_c}\left[\arcsin(\lambda_c-\lambda_d)+\frac{\pi}{2}-\alpha^4\arcsin\left(\frac{\lambda_c-\lambda_d}{\alpha}\right)-\frac{\pi}{2}\alpha^4\right]\\
&\quad +\frac{1}{4}\left(1-\frac{\lambda_d}{\lambda_c}\right)\left\{[2(\lambda_c-\lambda_d)^2-1]\sqrt{1-(\lambda_c-\lambda_d)^2}-[2(\lambda_c-\lambda_d)^2-\alpha^2]\sqrt{\alpha^2-(\lambda_c-\lambda_d)^2}\right\}
\end{aligned}
\tag{18}
$$

For the case Fig. 2c, we have:

$$
\begin{aligned}
n\pi(1-\alpha^2) &= \left(\frac{\lambda_d}{\lambda_c}+1\right)(\lambda_c+\lambda_d)(\sqrt{1-(\lambda_c+\lambda_d)^2}-\sqrt{\alpha^2-(\lambda_c+\lambda_d)^2})\\
&\quad + \left(\frac{\lambda_d}{\lambda_c}-1\right)(\lambda_c-\lambda_d)(\sqrt{1-(\lambda_c-\lambda_d)^2}-\sqrt{\alpha^2-(\lambda_c-\lambda_d)^2})\\
&\quad + \left(\frac{\lambda_d}{\lambda_c}+1\right)\left[\arcsin(\lambda_c+\lambda_d)-\alpha^2\arcsin\left(\frac{\lambda_c+\lambda_d}{\alpha}\right)\right]\\
&\quad + \left(\frac{\lambda_d}{\lambda_c}-1\right)\left[\arcsin(\lambda_c-\lambda_d)-\alpha^2\arcsin\left(\frac{\lambda_c-\lambda_d}{\alpha}\right)\right]\\
&\quad -\frac{2}{3\lambda_c}\left\{[1-(\lambda_c-\lambda_d)^2]^{3/2}-[1-(\lambda_c+\lambda_d)^2]^{3/2}-[\alpha^2-(\lambda_c-\lambda_d)^2]^{3/2}+[\alpha^2-(\lambda_c+\lambda_d)^2]^{3/2}\right\};
\end{aligned}
\tag{19}
$$

$$
\begin{aligned}
\frac{m\pi}{4}(1-\alpha^4) &= \frac{2}{3}\left(\frac{\lambda_d}{\lambda_c}+1\right)[(1-(\lambda_c+\lambda_d)^2)^{3/2}-(\alpha^2-(\lambda_c+\lambda_d)^2)^{3/2}]\\
&\quad +\frac{2}{3}\left(1-\frac{\lambda_d}{\lambda_c}\right)[(1-(\lambda_c-\lambda_d)^2)^{3/2}-(\alpha^2-(\lambda_c-\lambda_d)^2)^{3/2}]
\end{aligned}
$$

$$+\frac{1}{4\lambda_c}\left[\arcsin(\lambda_c-\lambda_d)+\arcsin(\lambda_c+\lambda_d)-\alpha^4\arcsin\left(\frac{\lambda_c-\lambda_d}{\alpha}\right)-\alpha^4\arcsin\left(\frac{\lambda_c+\lambda_d}{\alpha}\right)\right]$$
$$+\frac{1}{4}\left(1-\frac{\lambda_d}{\lambda_c}\right)\left\{[2(\lambda_c-\lambda_d)^2-1]\sqrt{1-(\lambda_c-\lambda_d)^2}-[2(\lambda_c-\lambda_d)^2-\alpha^2]\sqrt{\alpha^2-(\lambda_c-\lambda_d)^2}\right\}$$
$$+\frac{1}{4}\left(1+\frac{\lambda_d}{\lambda_c}\right)\left\{[2(\lambda_c+\lambda_d)^2-1]\sqrt{1-(\lambda_c+\lambda_d)^2}-\rightleftarrows[2(\lambda_c+\lambda_d)^2-\alpha^2]\sqrt{\alpha^2-(\lambda_c+\lambda_d)^2}\right\}$$

For the case Fig. 2d, we get:

$$n\pi(1-\alpha^2)=2\times\left(\arcsin\lambda_d-\alpha^2\arcsin\frac{\lambda_d}{\alpha}\right)+2\lambda_d(\sqrt{1-\lambda_d^2}-\sqrt{\alpha^2-\lambda_d^2})$$
$$\frac{m\pi}{4}(1-\alpha^4)=\frac{4}{3}[(1-\lambda_d^2)^{3/2}-(\alpha^2-\lambda_d^2)^{3/2}] \quad (20)$$

3.2. Load regime diagram

By substituting boundary curve Eqs. ①–⑥ into equilibrium conditions (18)–(20), we can get the boundary curves on *n*–*m* plane by using a numerical method. All the boundary curves form a load regime diagram for the pipe. The diagram for the case $\alpha = 0.95$ is shown in Fig. 7.

In Fig. 7, the load plane *n*–*m* is divided into seven regions: elastic region *E*, shakedown region S_1, cyclic plasticity region P_1, reverse plasticity region P_2, ratcheting regions R_1 and R_2, and plastic collapse region C_p.

The points *A* and *B* in Fig. 7 represent the elastic limit loads under axial force and bending moment, respectively, i.e. $N = N_e$ and $M = M_e$. Point *C* is the plastic limit load under bending moment. The value of *m* at *C* is called *section shape coefficient* β, which indicates the bending capacity of the beam. For pipe sections, β is equal to 1.27–1.7 when $\alpha = 1$–0, respectively. In Fig. 7, $\alpha = 0.95$ and $\beta = 1.3$. *D* is the intersection point of regions *S*, *P*, and *R*. By letting $c + d = R$ and $c = d$ simultaneously, we get $c = d = R/2$, and the coordinates of point *D* are:

$$n = 1-\frac{4(1-\alpha^3)}{3\pi(1-\alpha^2)};\quad m=1 \quad (21)$$

3.3. Polynomial fitting of curves in the load regime diagram

In the load regime diagram Fig. 7, curves ①–③ have analytical expressions as follows:

① $n + m = 1$

② $m = 1$

③ $m=\dfrac{3\pi(1-\alpha^2)(1-n)}{4(1-\alpha^3)}$

The curves ④–⑥ were obtained by numerical methods in order to give easy-to-use expressions for these curves, a polynomial fitting is performed. The general equation of polynomial regression is:

$$m = A + B_1\times n + B_2\times n^2 + B_3\times n^3 + \cdots \quad (22)$$

Fitting coefficients *A*, B_1, B_2, B_3, etc. are listed in Table 1.

Table 1
Results of polynomial regression for curves in the load regime diagram

Curve	Order	Parameter estimates	*R*-square	Standard deviation
④	3	$A = 1.0007$; $B_1 = 0.9318$; $B_2 = -2.7873$; $B_3 = 0.8540$	0.9999	7.5604E-4
⑤	2	$A = 1.3054$; $B_1 = -0.0047$; $B_2 = -2.1082$	1	1.8671E-4
⑥	4	$A = 1.3051$; $B_1 = 0.0077$; $B_2 = -1.6651$; $B_3 = 0.1339$; $B_4 = 0.2184$	1	1.7524E-4

By using the load regime diagram we can justify the elasto-plastic behavior of a pipe under given axial force n and bending moment m directly.

4. Summary

The boundary curve equations for various elasto-plastic behaviors of beams subjected to steady axial force and cyclic bending have been derived. The curves are obtained using two elasto-plastic characteristic parameters c and d. For a given cross-section, these curve equations can be calculated numerically and approximated by polynomial fitting. The load regime diagram for a pipe is obtained and plotted. This diagram indicates the elasto-plastic behavior of the pipe under a given combination of steady axial load and cyclic bending moment.

Acknowledgements

The study has been carried out as part of the "*Seismic Elasto-Plastic Analysis of Nuclear Piping Systems*" Program supported by the Nuclear Science Foundation of China with Grant Number Y7197EY506. The authors are sincerely grateful for the financial support.

References

Bree, J., 1967. Elastic–plastic behaviour of thin tubes subjected to internal pressure and intermittent high-heat fluxes with application to fast-nuclear-reactor fuel elements. J. Strain Anal. 2 (3), 226–238.

Bree, J., 1989. Plastic deformation of a closed tube due to interaction of pressure stresses and cyclic thermal stresses. Int. J. Mech. Sci. 31 (11/12), 865–892.

Gokhfeld, D.A., Cherniavsky, O.F., 1980. Limit Analysis of Structures at Thermal Cycling. Sijthoff and Noordhoff, Alphen an dem Rign, The Netherlands.

Hassan, T., Zhu, Y., Matzen, V.C., 1998. Improved ratcheting analysis of piping components. Int. J. Press. Vessels Piping 75, 643–652.

PVRC Subcommittee on Dynamic Stress Criteria, 1994. Alternative methods for the seismic analysis of piping systems. WRC Bull. 379, 1–39.

Scavuzzo, R.J., Lam, P.C., Gau, J.S., 1991. Experimental studies of ratcheting of pressurized pipe. ASME J. Press. Vessel Technol. 113, 210–218.

Scavuzzo, R.J., Lam, P.C., Gau, J.S., 1992. Ratcheting of pressurized piping subjected to seismic loading. ASME J. Press. Vessel Technol. 114, 315–320.

Slagis, G.C., 1991. Basis of current dynamic stress criteria for piping. WRC Bull. 367, 1–46.

Slagis, G.C., 1996. Experimental data on seismic response of piping. ASME Int. Conf. Press. Vessel Technol. 2, 481–487.

Tagart, S.W., Tang, Y.K., Guzy, D.J., Ranganath, S., 1990. Piping dynamic reliability and code rule change recommendations. Nucl. Eng. Des. 123, 373–385.

Webster, J.J., Hardy, S.J., Hyde, T.H., 1985. Inelastic behaviour of rectangular beams subjected to steady axial load and cyclic bending. Int. J. Mech. Sci. 27 (4), 257–271.

Yu, T.X., Johnson, W., 1982. Influence of axial force on the elastic–plastic bending and springback of a beam. J. Mech. Working Technol. 6, 5–21.